

# Properties of near-zero modes and chiral symmetry breaking

Christof Gattringer<sup>†</sup>, Meinulf Göckeler, P.E.L. Rakow,  
Stefan Schaefer and Andreas Schäfer

Institut für Theoretische Physik  
Universität Regensburg  
93040 Regensburg, Germany

## Abstract

We study localization and chirality properties of eigenvectors of the lattice Dirac operator. In particular we focus on the dependence of our observables on the size of the corresponding eigenvalue, which allows us to study the transition of a near-zero mode into a bulk mode. We analyze ensembles of quenched SU(3) configurations using a Dirac operator which is a systematic expansion in path length of a solution of the Ginsparg-Wilson equation. Our results support the interpretation of the excitations relevant for chiral symmetry breaking as interacting instantons and anti-instantons.

*To appear in Nuclear Physics B.*

PACS: 11.15.Ha

Key words: Lattice QCD, instantons, chiral symmetry breaking

---

<sup>†</sup> Supported by the Austrian Academy of Sciences (APART 654).

# 1 Introduction

Chiral symmetry breaking is one of the most intriguing features of QCD and the existence of a non-vanishing chiral condensate is a cornerstone in our understanding of hadron phenomenology. Analyzing and understanding the mechanisms which lead to the formation of the chiral condensate thus can provide deep insights into the nature of relevant excitations of QCD.

In the last 25 years a phenomenological picture of chiral symmetry breaking through the interaction of instantons and anti-instantons has been developed (see e.g. [1] for recent reviews). A single classical instanton or anti-instanton leads to a zero mode of the Dirac operator. An infinitely separated instanton anti-instanton pair has two zero modes, but as soon as the fermion wave functions start to overlap they mix, and the Dirac operator acquires a pair of small complex conjugate eigenvalues. As more instantons and anti-instantons are added they build up a non-vanishing density of eigenvalues near the origin. This non-vanishing density of eigenvalues in turn is related to the chiral condensate via the Banks-Casher relation [2].

This picture of chiral symmetry breaking through instantons provides a wealth of signatures for the properties of the eigenvectors of the Dirac operator with eigenvalues close to 0, the so-called *near-zero modes*. In particular they should have pronounced localization and chirality properties. These signatures can be directly tested in an ab-initio calculation using lattice gauge theory. The recent progress in understanding chiral symmetry on the lattice based on the Ginsparg-Wilson relation [3] now allows us to probe the QCD vacuum with a Dirac operator which respects chiral symmetry. Analyzing properties of eigenvectors of the Dirac operator to learn about instantons is a more direct approach than analyzing the gauge fields with cooling methods. The eigenvectors directly reflect the relevant excitations as seen by the Dirac operator without introducing a filtering process by hand. Further evidence for the dominance of instantons has been obtained by showing that fermionic  $n$ -point functions can be saturated using spectral decomposition with only the lowest eigenmodes of the lattice Dirac operator [4, 5, 6].

Let us stress that while the instanton anti-instanton scenario of chiral symmetry breaking is highly popular, it is still far from being established. For an alternative based on monopole physics see e.g. [7] and references therein. Thus detailed numerical tests based on chirally improved lattice calculations are highly appropriate.

In this article we present our results for locality and chirality properties of eigenvectors of the lattice Dirac operator. In particular we also focus on the

dependence of our observables on the size of the corresponding eigenvalue. This allows us to study how localization and chirality of a near-zero mode change as the corresponding eigenvalue moves into the bulk of the spectrum. We analyze ensembles of quenched SU(3) configurations for different lattice sizes and three values of the gauge coupling. We use a Dirac operator which is a systematic approximation of a solution of the Ginsparg-Wilson equation. It has very good chiral properties and is numerically cheaper than an exact solution of the Ginsparg-Wilson equation such as e.g. the overlap operator. Our results clearly support the interpretation of the excitations relevant for chiral symmetry breaking as interacting instantons and anti-instantons.

The article is organized as follows: In the next section we collect technical preliminaries, in particular we discuss our gauge ensembles, the Dirac operator we use and the details of the diagonalization. This is followed by sections where we discuss our results for the spectral density (Section 3) of the Dirac operator and for the localization properties of its eigenvectors (Section 4). In Section 5 we analyze the chirality properties of the near-zero modes. The article closes with a summary of our results.

## 2 Technical remarks

**Gauge configurations:** We use ensembles of SU(3) gauge fields in the quenched approximation generated with the Lüscher-Weisz action [8, 9]. In addition to the standard plaquette term with coefficient  $\beta_1$  this action also contains a rectangle term with coefficient  $\beta_2$  and a parallelogram term with coefficient  $\beta_3$  (see [9] for a detailed discussion of the action). The coefficient  $\beta_1$  is an independent parameter, while  $\beta_2$  and  $\beta_3$  can be computed from  $\beta_1$  using e.g. tadpole improved perturbation theory [9, 10]. We use  $\beta_1 = 8.10, 8.30$  and  $8.45$ . The corresponding values of  $\beta_2$  and  $\beta_3$  were determined in [11]. We performed runs on lattices of size  $8^4$ ,  $12^4$  and  $16^4$  and the statistics for our ensembles is given in Table 1. We use a mix of Metropolis and over-relaxation steps to update the gauge fields. In order to set the scale we computed the Sommer parameter [12]  $r_0$  for the  $16^4$  ensembles. We give our results for  $r_0/a$  together with the lattice spacing  $a$  (assuming  $r_0 = 0.5$  fm) in Table 1.

**Dirac operator:** Our Dirac operator  $D$  is a systematic expansion of a solution of the Ginsparg-Wilson equation [3],

$$\gamma_5 D + D \gamma_5 = D \gamma_5 D. \quad (1)$$

	$\beta_1 = 8.10$	$\beta_1 = 8.30$	$\beta_1 = 8.45$
$r_0/a$	3.94(16)	4.67(13)	5.00(5)
$a$	0.127(5) fm	0.107(3) fm	0.100(1) fm
$8^4$	800	800	800
$12^4$	400	400	400
$16^4$	200	200	200

Table 1: Sommer Parameter  $r_0$ , lattice spacing  $a$  and statistics for our gauge field ensembles.

It has been understood during the last few years, that solutions of (1) can be used to implement chiral symmetry on the lattice. The two known<sup>1</sup> exact solutions are perfect actions [13, 14] and overlap fermions [15]. In a series of recent publications [11, 16, 17, 18] it has been demonstrated that for many problems it is sufficient to work with an approximate solution of (1) which is considerably cheaper from a numerical point of view. The idea [18] is to expand the most general Dirac operator  $D$  on the lattice into a sum of simple operators. Each of these simple operators is built from a set of paths of the same length. The members of these sets are related by symmetry transformations as e.g. rotations, reflections etc. Along each path one builds a gauge transporter from the link variables and multiplies it with a Kronecker symbol with the endpoints of the path as arguments. The most general Dirac operator is then obtained by multiplying this object with an element of the Clifford algebra and summing all the resulting simple lattice operators with some real coefficients [14, 18].

Once the expansion of the most general Dirac operator is established it can be inserted into the Ginsparg-Wilson equation. The left hand side can be evaluated easily by commuting the Clifford algebra elements in the expansion with  $\gamma_5$ . The right hand side amounts to a commutation with  $\gamma_5$  and multiplications of the individual terms in the expansion of  $D$ . It can be shown [18] that the product of any two terms of our expansion which appears on the right hand side of (1) gives a term which is already present in the full expansion of  $D$ , i.e. shows up also on the left hand side of (1). The coefficients in front of the individual terms on both sides of (1) have to be equal. This results in a system of coupled quadratic equations which can be solved numerically. In [16] an approximate solution with 19 terms was constructed and analyzed. We use the same solution here. A detailed

---

<sup>1</sup>We remark that when one adds a fifth dimension also the domain wall fermions provide a solution of the Ginsparg-Wilson equation.

description of the terms as well as the coefficients can be found in the appendix of [11]. Our expansion of a solution of the Ginsparg-Wilson equation is an expansion in terms of path length, since the size of the coefficients multiplying each term in the expansion decreases as the length of the paths increases [16].

The symmetries that are implemented and are responsible for grouping the paths into the above mentioned sets are lattice translations and lattice rotations as well as parity, charge conjugation and  $\gamma_5$ -hermiticity, where  $\gamma_5$ -hermiticity is defined as

$$D \gamma_5 = \gamma_5 D^\dagger . \quad (2)$$

The property (2) can be seen [14, 18] to correspond to the properties of  $D$  which are used to prove CPT in the continuum. Eq. (2) has an important implication for the  $\gamma_5$ -matrix element of the eigenvectors of  $D$ . Let  $\psi$  be such an eigenvector, i.e.  $D\psi = \lambda\psi$ . Then a few lines of algebra show that [19]

$$\psi^\dagger \gamma_5 \psi = 0 \ , \ \text{unless } \lambda \text{ is real} \ . \quad (3)$$

This equation is the basis for the identification of topological modes. For the continuum Dirac operator and for a  $D$  which is an exact solution of the Ginsparg-Wilson equation one has exact zero modes. Only zero modes have a non-vanishing matrix element with  $\gamma_5$ . Here we are working with an approximate solution of the Ginsparg-Wilson equation and we do not have exact zero modes. However, eigenvectors for which the corresponding eigenvalue has a non-vanishing imaginary part cannot be candidates for zero modes, since their matrix elements with  $\gamma_5$  vanish exactly. In our approximation the topological modes show up as eigenvectors with a small real eigenvalue. For the real eigenvalues on the  $16^4$  lattices we find mean values of 0.0124, 0.0122 and 0.0095 for  $\beta_1 = 8.10$ ,  $\beta_1 = 8.30$  and  $\beta_1 = 8.45$  respectively. The distributions (see [20]) of the real eigenvalues are very narrow and we find that 95% of the real eigenvalues lie between 0 and 0.05. The matrix elements  $\psi^\dagger \gamma_5 \psi$  typically have a value  $\sim \pm 0.8$ . If one added more terms in our approximation then the real modes would be closer to 0 and the matrix element with  $\gamma_5$  closer to  $\pm 1$ .

**Computation of the eigenvalues:** For the computation of the eigenvalues and eigenvectors we used the implicitly restarted Arnoldi method [21]. For lattice sizes  $8^4$  and  $12^4$  we computed 50 eigenvalues and the corresponding eigenvectors for each of our gauge field configurations and 30 eigenvalues and eigenvectors for the ensembles on the  $16^4$  lattice. The search criterion

for the eigenvalues was their modulus, i.e. we computed eigenvalues in concentric circles around the origin until 50, respectively 30 were found. The boundary conditions for the fermions were periodic in the space directions and anti-periodic in time.

### 3 Density of eigenvalues

When describing chiral symmetry breaking based on instanton phenomenology, a major ingredient is the Banks-Casher formula [2] which relates the density  $\rho(\lambda)$  of eigenvalues  $\lambda$  at the origin to the chiral condensate,

$$\langle \overline{\psi}\psi \rangle = -\pi \rho(0) V^{-1}. \quad (4)$$

We use a convention for the density  $\rho(\lambda)$  such that  $\rho(\lambda) \Delta\lambda$  gives the number of eigenvalues in the interval  $\Delta\lambda$ . The second ingredient for chiral symmetry breaking through instantons is the above mentioned interaction of pairs of instantons and anti-instantons which leads to a pair of small complex conjugate eigenvalues. In the chirally broken phase of QCD the abundance of interacting instantons and anti-instantons builds up a finite density of eigenvalues near the origin thus leading to a non-vanishing chiral condensate. This picture provides a wealth of signatures for the eigenvectors of the Dirac operator with small eigenvalues, the near-zero modes.

Before we discuss our tests of some of these characteristic features of the near-zero modes we briefly present our results for the density of eigenvalues. For the continuum Dirac operator the spectrum is restricted to the imaginary axis and the definition of the spectral density is straightforward. For a solution of the Ginsparg-Wilson equation (1) the spectrum is located on a circle of radius 1 with center 1 in the complex plane. For our approximate solution  $D$  of (1) the spectrum fluctuates slightly around this circle (compare e.g. the spectra shown in [11]). The non-vanishing real parts of the eigenvalues of an exact or approximate Ginsparg-Wilson fermion require a small modification in the definition of the eigenvalue density  $\rho(\lambda)$ . We bin the eigenvalues with respect to their imaginary part and count the number of eigenvalues in each bin. Eigenvalues with vanishing imaginary part, i.e. the zero modes, were left out. After dividing the count in each bin by the total number of eigenvalues we obtain the histograms for  $\rho(\lambda)$  used in Fig. 1 below. Since we are only interested in the density  $\rho(\lambda)$  in a region of  $\lambda$  where the real parts of the eigenvalues on the Ginsparg-Wilson circle are small, binning with respect to the imaginary parts of  $\lambda$  gives a good approximation of the continuum definition of the spectral density.

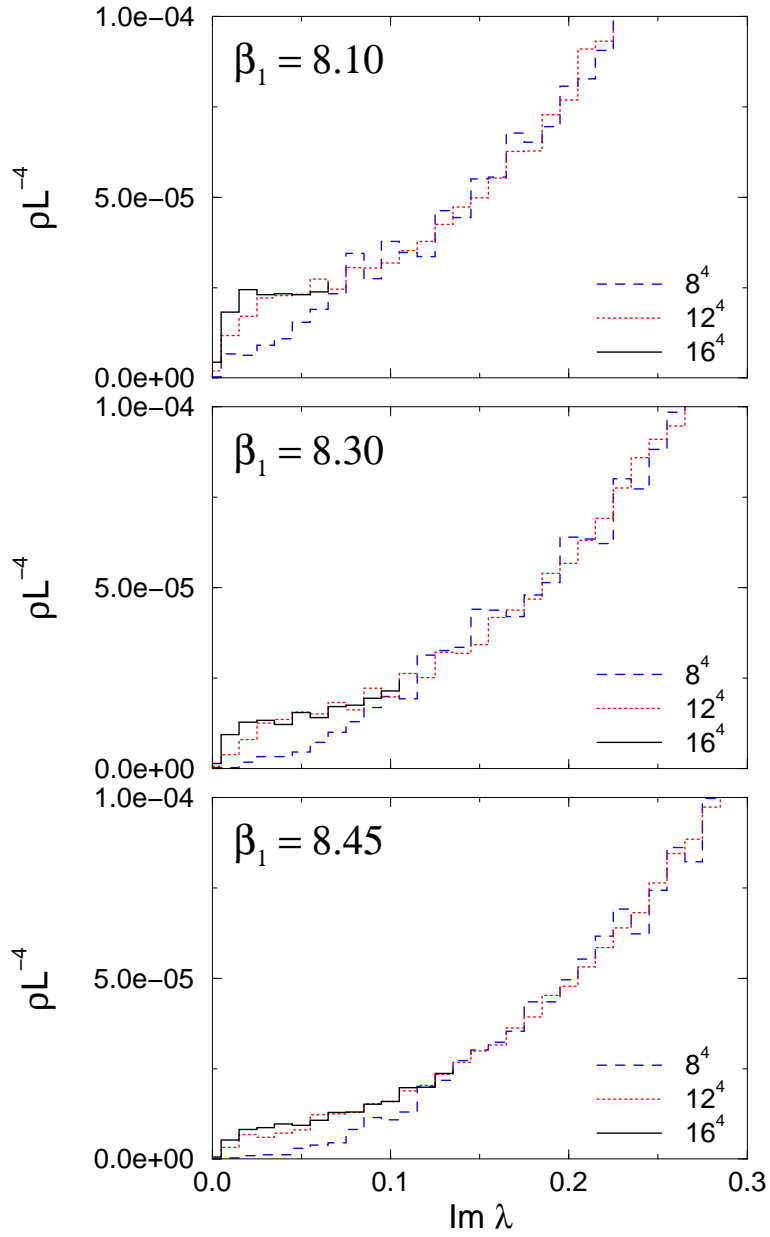


Figure 1: Density of eigenvalues as a function of  $\text{Im } \lambda$ . The density is normalized by the inverse volume of the corresponding lattices. Zero modes were left out for the evaluation of the density.

In Fig. 1 we show our results for the density of eigenvalues. We use the spectra for  $\beta_1 = 8.10$  (top plot),  $\beta_1 = 8.30$  (middle plot) and  $\beta_1 = 8.45$  (bottom plot) and display the results for all three volumes  $8^4$  (dashed curve)  $12^4$  (dotted curve) and  $16^4$  (full curve). We remark that for the largest lattice ( $16^4$ ) the smallest Matsubara frequency has a value of  $\pi/16 = 0.1963$ , such that many of the eigenvalues are considerably below the smallest eigenvalue for the free case. We plot the density  $\rho(\lambda)$  normalized by the volume  $L^4$  as a function of  $\text{Im } \lambda$  where, since the curve is symmetric with respect to reflection at the origin, we display only positive  $\text{Im } \lambda$ . One finds that the data for the density essentially fall on universal curves. Only near the origin the density is more rounded for the smaller lattices in agreement with universal random matrix theory predictions [22]. For the same reason also the curve for the largest system ( $16^4$ ) still shows a drop near the origin. Up to this finite-size effect, the density remains non-zero down to  $\lambda = 0$ , thus building up the chiral condensate according to the Banks-Casher formula (4). We remark that at  $\beta_1 = 8.45$  the smallest lattice ( $8^4$ ) already is in the deconfined phase, i.e. there the density develops a gap (compare [11]). It is obvious that for  $\beta_1 = 8.10$ , i.e. the ensemble with the largest value of the gauge coupling the density of eigenvalues and thus the condensate is largest while it becomes smaller with increasing  $\beta_1$ .

We remark that in a recent study [23] of quenched QCD at finite temperature using the overlap operator, a small nonvanishing density of eigenvalues near the origin was found even in the deconfined phase. In our recent paper [11] with the ultralocal, chirally improved operator no statistically significant signal for a nonvanishing density in the deconfined phase was seen. This discrepancy might be related to an observation we made recently [24]. For smooth instantons on the lattice the large extent of the overlap operator considerably distorts the zero modes for instantons with radius  $\leq 2.5$  in lattice units, i.e. objects with a diameter of  $\leq 5.0$ . We thus suspect that using the overlap operator on lattices with time extent 4 (as in [23]) may lead to serious finite size effects.

## 4 Localization properties

Let us now come to the analysis of the characteristic features of the near-zero modes, i.e. the eigenvectors of the Dirac operator with small eigenvalues. In order to develop these characteristic features we first discuss the behavior of exact zero modes in the continuum. For an instanton configuration in the continuum, the Dirac operator has an exact zero mode  $\psi$  which is localized



in space-time around the center of the instanton and this localization has a radius proportional to that of the underlying instanton. A gauge invariant density which displays this localization is obtained by summing  $|\psi(x, d, c)|^2$  over the Dirac and color indices  $d$  and  $c$  at each space-time point  $x$  individually. A lattice discretization of this scalar density  $p(x)$  is given by

$$p(x) = \sum_{c,d} \psi(x, c, d)^* \psi(x, c, d) , \quad (5)$$

where now  $\psi(x, c, d)$  are the entries of the eigenvectors of our lattice Dirac operator  $D$ . As expected from the analytic result in the continuum, this density shows a clear localization at the position of an isolated smooth instanton put on the lattice by hand [24, 25]. We remark that since the eigenvectors  $\psi$  of  $D$  are normalized one has

$$\sum_x p(x) = 1 . \quad (6)$$

A zero mode of the continuum Dirac operator is also an eigenstate of  $\gamma_5$ . Hence it is interesting to also analyze the gauge invariant pseudoscalar density  $p_5(x)$  defined by

$$p_5(x) = \sum_{c,d,d'} \psi(x, c, d)^* (\gamma_5)_{d,d'} \psi(x, c, d') . \quad (7)$$

When evaluating the corresponding continuum quantity for a zero mode,  $p_5(x)$  differs from its scalar counterpart only by a possible sign, i.e. the scalar density equals the pseudoscalar density for an instanton but the two densities have opposite sign for an anti-instanton. If one puts a smooth instanton anti-instanton pair on the lattice by hand the density of the corresponding near-zero mode shows a *dipole behavior*. Near the instanton peak of the pair  $p_5(x)$  is positive while it is negative near the center of the anti-instanton. When analyzing the densities  $p(x)$  and  $p_5(x)$  for thermalized configurations one still finds localized structures and also dipole structures which can be interpreted as signatures of isolated instantons or instanton anti-instanton pairs (see e.g. [11] for plots of examples). Using cooling techniques to identify the instantons independently it has been found that the localization of the eigenvectors is concentrated at the same region where the cooling procedure finds an instanton (see e.g. [6]).

In order to go beyond analyzing the localization properties of the eigenvectors by merely inspecting plots of the scalar density it is convenient to

introduce the scalar inverse participation ratio  $I$ , which is widely used in solid state physics,

$$I = V \sum_x p(x)^2. \quad (8)$$

$V$  denotes the volume  $L^4$ . From its definition in Eq. (5) it follows that  $p(x) \geq 0$  for all  $x$ . Taking into account the normalization Eq. (6) one finds that a maximally localized eigenvector which has support on only a single site  $x'$  must have  $p(x) = \delta_{x,x'}$ . Inserting this into the definition (8) for the inverse participation ratio one finds that a maximally localized eigenvector has  $I = V$ . Conversely, a maximally spread eigenvector has  $p(x) = 1/V$  for all  $x$ . In this case, the inverse participation ratio gives a value of  $I = 1$ . Thus  $I$  has a high value for localized states while  $I$  is small for delocalized ones. An alternative measure for the localization of the eigenvectors, based on their self correlation has been studied in [5].

We now use the inverse participation ratio to analyze the localization of the near-zero modes. According to the instanton picture the small eigenvalues come from interacting instantons and anti-instantons. If an instanton and an anti-instanton are infinitely far apart, i.e. they do not interact, the Dirac operator still sees them as two independent objects and displays two eigenvalues 0. As soon as the two objects interact this degeneracy is lifted and the two eigenvalues split into a pair of small complex conjugate eigenvalues. When the instanton and the anti-instanton approach further, the two eigenvalues move further up (down) in imaginary direction. At the same time the instanton and the anti-instanton start to annihilate. The localization is washed out and the corresponding eigenvalues end up in the bulk of the spectrum. Thus one expects that for eigenvalues very close to the origin the localization is still large since the two partners remain relatively unperturbed. On the other hand eigenvalues further up (down) the imaginary axis come from pairs where the partners are already relatively close to each other and should be less localized.

In Fig. 2 we plot our results for the average  $\langle I \rangle$  of the inverse participation ratio as a function of  $\text{Im } \lambda$ . The histograms were obtained by binning  $\text{Im } \lambda$  and computing the average of  $I$  for the eigenvectors with eigenvalues in each bin. Topological modes, i.e. modes with small real eigenvalues were left out in the computation of the histograms<sup>2</sup>. Since the distribution is symmetric with respect to the origin we display the curves only for  $\text{Im } \lambda > 0$ . We

---

<sup>2</sup>We remark that the topological modes have values of  $I$  varying between 1.8 and up to 100, with the highest values of  $I$  coming from defects. The distribution is peaked near small values similar to the distribution for the near zero modes shown in Fig. 3.

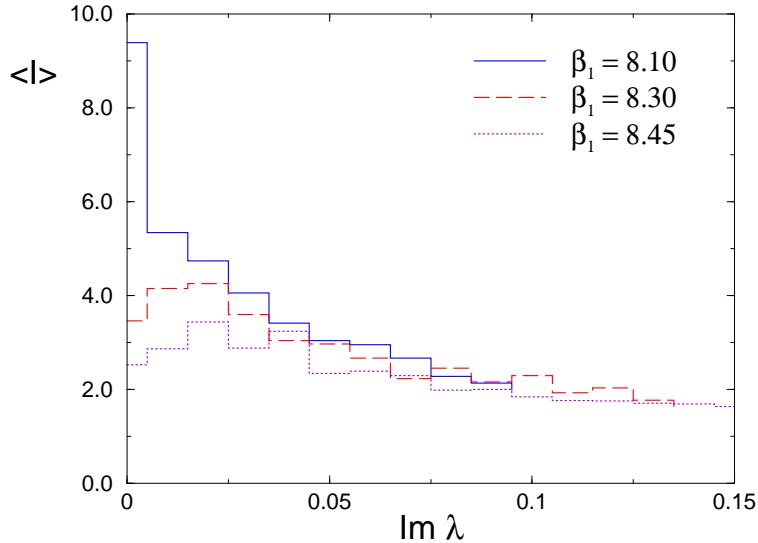


Figure 2: The average inverse participation ratio  $\langle I \rangle$  of the near-zero modes as a function of  $\text{Im } \lambda$  for lattice size  $16^4$ . We remark that in the first bin real modes were left out.

show our results for the  $16^4$  lattice at all three values of  $\beta_1$ . All three curves display their maximum at or near the origin, as expected from the picture of interacting instantons and anti-instantons. The same behavior was observed for the near-zero modes of the staggered Dirac operator in [26]. Furthermore the eigenvectors for the  $\beta_1 = 8.10$  ensembles have the largest average of  $I$  near  $\lambda = 0$  while the eigenvectors for  $\beta_1 = 8.45$  have the smallest values. This poses an interesting question: Is it simply a larger number of localized states which leads to a larger condensate for  $\beta_1 = 8.10$ , or do in addition also the near zero modes themselves become more localized? This question can be analyzed by studying the probability distribution of the inverse participation ratio.

In Fig. 3 we show the probability distribution  $P(I)$  of the inverse participation ratio for the near-zero modes (no zero modes were taken into account). More precisely, we show the probability distribution for all eigenvectors with eigenvalues obeying  $0 < |\text{Im } \lambda| \leq 0.05$ , i.e. for those modes for which the curves in Fig. 2 show a strong  $\beta_1$  dependence. The distributions  $P(I)$  are normalized such that their integral over  $I$  equals 1. It is obvious from Fig. 3, that for  $\beta_1 = 8.10$  the distribution is shifted towards larger

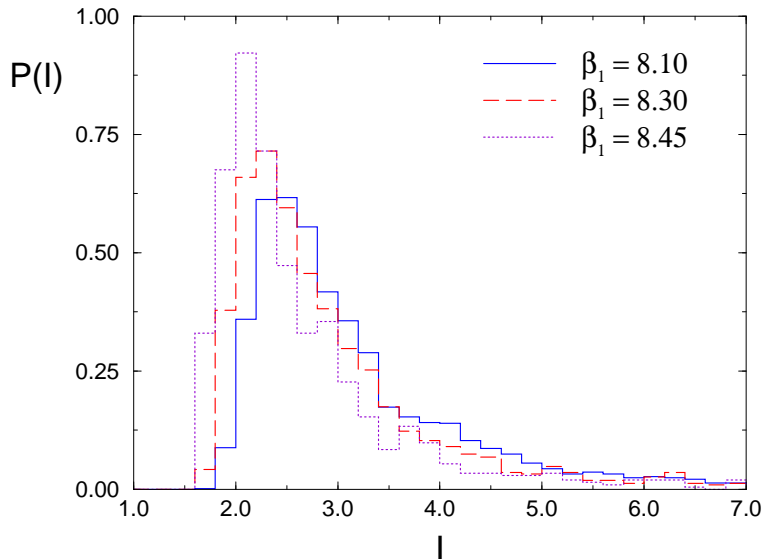


Figure 3: Distribution of the inverse participation ratio for the near-zero modes with  $0 < |\text{Im } \lambda| \leq 0.05$ .

values of  $I$ , while it moves towards smaller values of  $I$  as  $\beta_1$  is increased. Thus not only the average  $\langle I \rangle$  of the inverse participation ratio is larger for smaller  $\beta_1$ , but also the probability of finding a localized mode increases with smaller  $\beta_1$ .

So far we have only concentrated on the localization of the near-zero modes. According to the instanton picture of chiral symmetry breaking also their local chiral behavior should have an interesting signature. In particular  $p_5(x)$  should have positive sign near instanton peaks and negative sign near anti-instanton peaks. In the next section we will discuss an observable introduced in [27] which tests the local chirality for each lattice point individually. Before we come to our results for the local chirality let us first look at an observable which is a global measure for the chirality of an eigenvector.

Similarly to the scalar inverse participation ratio  $I$  of Eq. (8) we can also define a measure  $I_5$  for the localization of the pseudoscalar density  $p_5(x)$  (see Eq. (5)),

$$I_5 = V \sum_x p_5(x)^2. \quad (9)$$

Let us discuss the behavior of  $I_5$  for a smooth instanton and a smooth

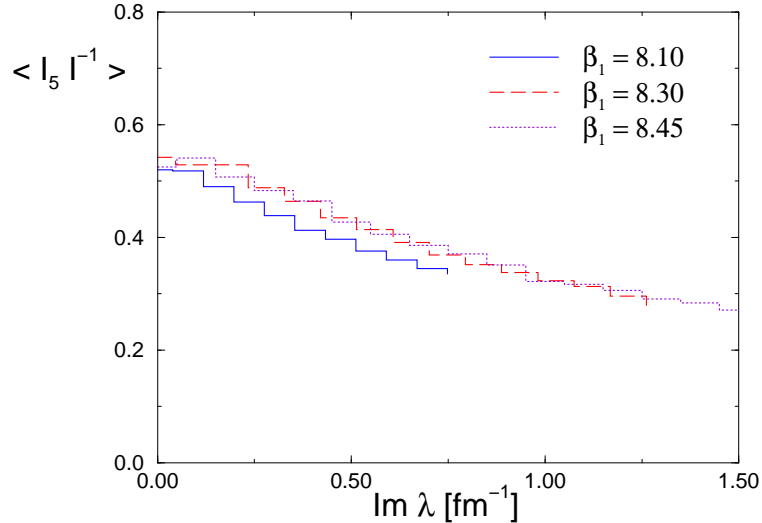


Figure 4: The ratio  $I_5/I$  of pseudoscalar and scalar inverse participation ratio as a function of  $\text{Im } \lambda$  (in physical units). The data were computed on the  $16^4$  lattices.

instanton anti-instanton pair. For a zero mode, corresponding to a single smooth instanton or anti-instanton, one has  $I = I_5$  since for all  $x$  the  $p(x)$  differ from the  $p_5(x)$  only by a global sign. For an instanton anti-instanton pair the pseudoscalar density  $p_5(x)$  has to undergo a change of sign, since for  $x$  near the instanton peak  $p_5(x)$  is positive while it is negative near the center of the anti-instanton. This implies that  $p_5(x)$  has to go through 0 for some  $x$ . Since (compare the definitions (5),(7)) for each  $x$  we have  $|p_5(x)| \leq p(x)$ , it follows from the definitions of  $I$  and  $I_5$  that for an instanton anti-instanton pair one has  $I_5 < I$ . As long as the two constituents are relatively remote from each other and much of their identity as an independent instanton, respectively anti-instanton remains intact one still finds  $I_5 \sim I$ . However, for pairs where the partners are close to each other, one expects values of  $I_5$  considerably smaller than  $I$ . Thus one expects to find a relatively large ratio of  $I_5/I$  for modes with eigenvalues very close to the origin and a drop of this ratio as  $|\text{Im } \lambda|$  increases.

In Fig. 4 we show our results for the average  $\langle I_5/I \rangle$  as a function of  $\text{Im } \lambda$ . Again we do not take into account zero modes. One clearly sees the drop of  $\langle I_5/I \rangle$  as  $\text{Im } \lambda$  increases. This is in agreement with the above discussed

picture of instanton anti-instanton pairs where the two partners lose their chiral identity as they approach each other. Note that the curves for the three different values of  $\beta_1$  are very similar.

## 5 Local chirality

To further study the nature of the near-zero modes we analyze the local chirality observable proposed by Horváth et al. in [27]. In the original article [27] the computation was done with Wilson fermions and the result was interpreted as evidence against the instanton picture. In the meantime the local chirality variable was reanalyzed in several articles [28] using different Dirac operators or a modification of the observable. These latter collaborations all interpret their results in favor of the instanton picture. Here we add further supporting evidence by analyzing for the first time how the local chirality of a near-zero mode changes as  $|\text{Im } \lambda|$  of the corresponding eigenvalue increases. This allows us to directly see how an instanton and an anti-instanton lose their chirality and the corresponding near-zero mode turns into a bulk mode.

Before we present our numerical results we briefly repeat the definition of the local chirality variable of [27]. In analogy to the densities  $p(x)$  and  $p_5(x)$  of Eqs. (5),(7) we can define local densities  $p_+(x)$  and  $p_-(x)$  with positive and negative chirality,

$$p_{\pm}(x) = \sum_{c,d,d'} \psi(x, c, d)^* (P_{\pm})_{d,d'} \psi(x, c, d') , \quad (10)$$

where  $P_{\pm}$  denote the projectors onto positive and negative chirality  $P_{\pm} = (1 \pm \gamma_5)/2$ . It is now interesting to analyze locally for each lattice point  $x$  the ratio  $p_+(x)/p_-(x)$ . For a classical instanton in the continuum, the corresponding zero mode  $\psi(x)$  has positive chirality and the density  $p_+(x)$  is positive for all  $x$  while  $p_-(x)$  vanishes everywhere. Thus the ratio of the two always gives  $\infty$ . For an anti-instanton the roles of  $p_+$  and  $p_-$  are exchanged and the ratio is always 0. When now analyzing the eigenvectors for an interacting instanton anti-instanton pair this property should still hold approximately near the peaks. The ratio  $p_+(x)/p_-(x)$  is expected to be large for all  $x$  near the instanton peak of the pair and small for all  $x$  near the anti-instanton peak. In a final step Horváth et al. map the two extreme values  $\infty$  and 0 of the ratio  $p_+(x)/p_-(x)$  onto the two values  $+1, -1$  using the arctangent. One ends up with the local chirality variable  $X(x)$  defined as

$$X(x) = \frac{4}{\pi} \arctan \left( \sqrt{\frac{p_+(x)}{p_-(x)}} \right) - 1. \quad (11)$$

If the eigenvectors for the near-zero eigenvalues correspond to instanton anti-instanton pairs then the values of  $X(x)$  should cluster near  $+1$  and  $-1$  when one selects lattice points  $x$  near the peaks of the scalar density  $p(x)$ . One can choose different values for the percentage of points  $x$  used for the average and here we will present results for cuts of 1%, 6.25% and 12.5%. This means that we average over those 1% (6.25%, 12.5%) of all lattice points which support the highest peaks of  $p(x)$ . The smallest cut-off of 1% will give the best signature since only the highest peaks which are not so much affected by quantum fluctuations contribute. On the other hand for such a small cut-off the results are not expected to be very conclusive, since typically instanton models have a packing fraction of instantons considerably larger than 1% (see [1]). As already announced, we study the dependence of the chiral density of the eigenvectors on the imaginary part  $\text{Im } \lambda$  of the corresponding eigenvalues. To do so we bin  $\text{Im } \lambda$  and sum the contributions  $X(x)$  for each bin individually. In order to compare the different bins we normalize  $X(x)$  such that the area under the histogram is 1 for each of the  $\lambda$ -bins.

In Fig. 5 we show our results for the  $\beta_1 = 8.10$  ensemble on the  $16^4$  lattice and Fig. 6 displays the local chirality for  $\beta_1 = 8.45$ . The top plots give the result for the 1% cut on the number of supporting lattice points, while the middle and bottom plots are for 6.25% and 12.5% respectively. We remark that due to the higher density of eigenvalues  $\lambda$  at  $\beta_1 = 8.10$  our data which were computed from the eigenvectors corresponding to the 30 lowest eigenvalues extend only to  $|\text{Im } \lambda| = 0.1$  while we reach  $|\text{Im } \lambda| = 0.15$  at  $\beta_1 = 8.45$ . It is obvious, that for all plots the modes with eigenvalues closest to 0 have the best signal for local chirality, i.e. the curves in the first bin always show two well pronounced maxima in the vicinity of  $\pm 1$  and a clear valley separating the two peaks. As  $|\text{Im } \lambda|$  increases, the signal for local chirality weakens, i.e. the valley is less pronounced and the height of the peaks lowers. This reflects the washing out of the local chirality as instantons and anti-instantons approach, as discussed above. The same effect has been observed for the global observable  $\langle I_5/I \rangle$  as shown in Fig. 4. Thus, as a near-zero mode turns into a bulk mode it loses its local chirality.

When comparing the results for the different cuts on the percentage of the supporting lattice points one finds, as expected, that the strongest signal for local chirality is obtained for the 1%-cut where only the highest peaks

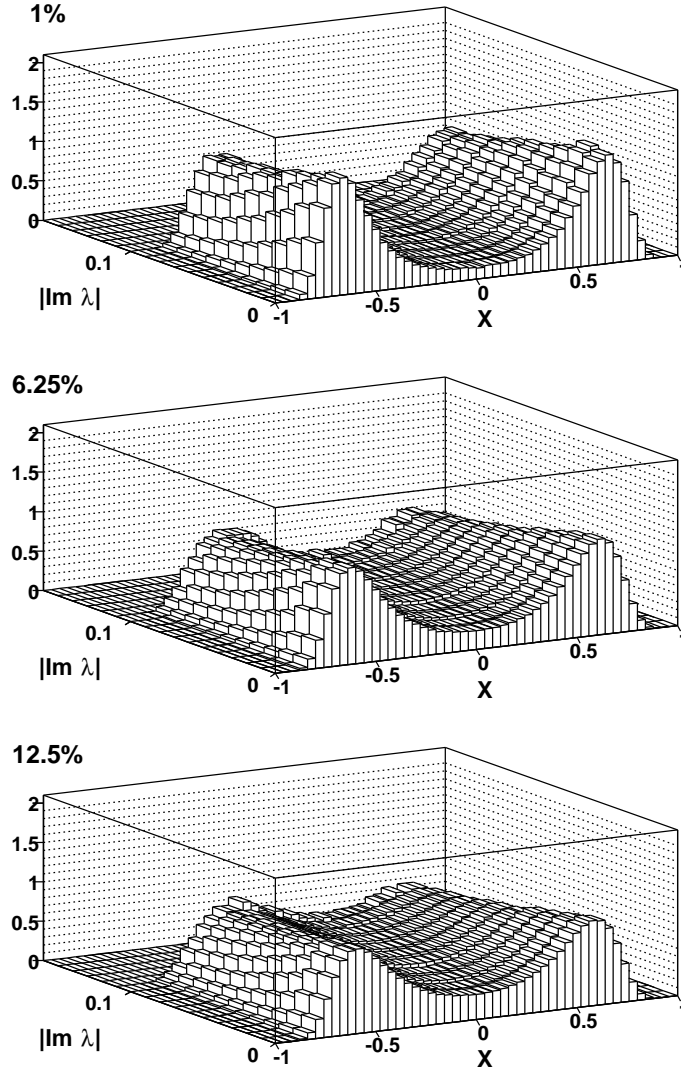


Figure 5: Local chirality for the near-zero modes in the  $\beta_1 = 8.10$  ensemble on the  $16^4$  lattices. We binned the data with respect to the imaginary part  $|\text{Im } \lambda|$  of the eigenvalues and normalized the histograms to 1 for each  $\lambda$ -bin individually. We use cuts of 1% (top plot), 6.25% (middle plot) and 12.5% (bottom plot) for the percentage of supporting lattice points.



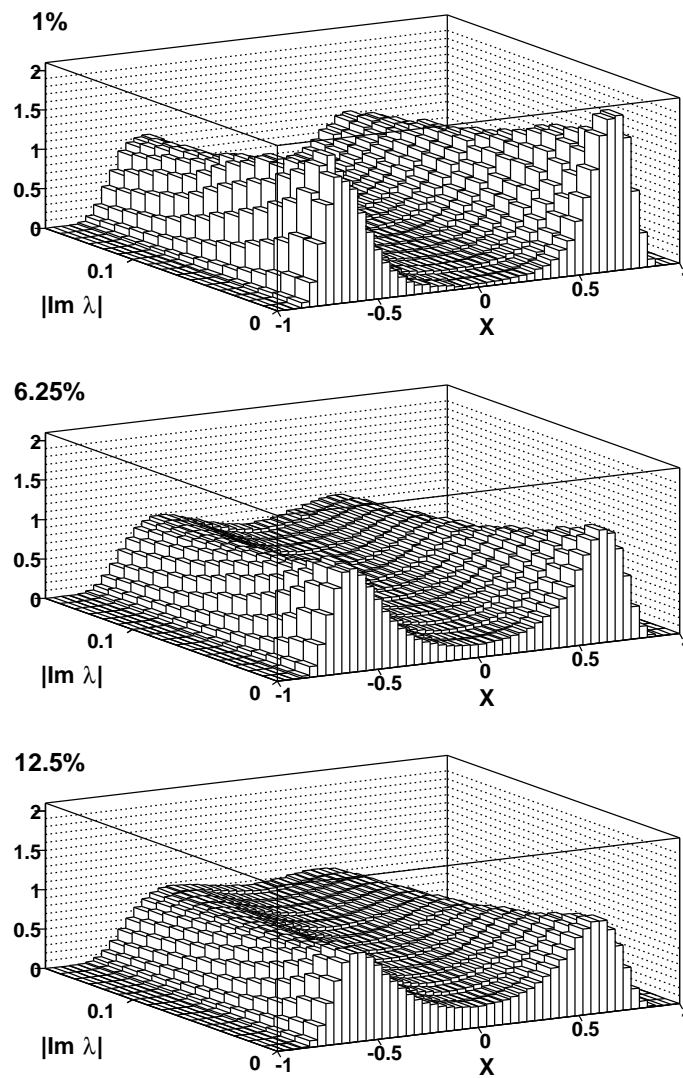


Figure 6: Local chirality for the near-zero modes as in Fig. 5 but now for  $\beta_1 = 8.45$ .

are taken into account. However, also for cuts of 6.25% and 12.5% one still finds a clear signal for local chirality. Finally when comparing the results for the two different values of  $\beta_1$  we observe in the  $\beta_1 = 8.45$  ensemble a better signal of local chirality for the modes with eigenvalues very close to 0. This can be understood by the stronger suppression of quantum fluctuations at larger values of  $\beta_1$ .

## 6 Summary

In this article we have studied localization and chirality properties of eigenvectors of the lattice Dirac operator with small eigenvalues. According to the picture of chiral symmetry breaking through instantons these near-zero modes should display characteristic features. In particular, since they are supposed to trace interacting instantons and anti-instantons, they are expected to be relatively localized and their pseudoscalar density should display dipole behavior. We analyze these modes using the scalar and pseudoscalar participation ratio and the local chirality variable of Horváth et al. In particular we focus on the dependence of these observables on the imaginary parts  $\text{Im } \lambda$  of the corresponding eigenvalues. One expects that both the locality and the local chirality of the near-zero modes decrease with increasing  $|\text{Im } \lambda|$ . Our main findings are as follows:

- When plotting the average inverse participation ratio  $\langle I \rangle$  as a function of  $\text{Im } \lambda$ , we find the largest values of  $\langle I \rangle$  near the origin and  $\langle I \rangle$  decreases as  $|\text{Im } \lambda|$  increases.
- A comparison of the probability distribution  $P(I)$  of the inverse participation ratio for the near-zero modes shows that for the strongest gauge coupling (i.e.  $\beta_1 = 8.10$ ), where the chiral condensate is biggest, one has the largest probability of finding localized states.
- A plot of the average ratio  $\langle I_5/I \rangle$  as a function of  $\text{Im } \lambda$  shows that the most chiral states are located near the origin and as  $|\text{Im } \lambda|$  is increased this chirality becomes washed out. We observe that the ratio  $\langle I_5/I \rangle$  falls on a universal curve for the different values of  $\beta_1$ , i.e. is relatively stable under quantum fluctuations.
- The observable of Horváth et al. gives a clear signal for local chirality for cuts of 1%, 6.25% and 12.5% on the number of supporting lattice points. When  $|\text{Im } \lambda|$  is increased we observe a decay of the local chirality for the corresponding modes.

Our results support the picture of the emergence of the chiral condensate through the interaction of instantons and anti-instantons.

**Acknowledgements:** We would like to thank Peter Hasenfratz, Holger Hehl, Ivan Hip, Christian B. Lang, Ferenc Niedermayer, Edward Shuryak, Wolfgang Söldner, Christian Weiss and Vladimir I. Zakharov for interesting discussions. This project was supported by the Austrian Academy of Sciences, the DFG and the BMBF. We thank the Leibniz Rechenzentrum in Munich for computer time on the Hitachi SR8000 and their operating team for training and support.

## References

- [1] T. Schäfer and E.V. Shuryak, Rev. Mod. Phys. 70 (1998) 323; D. Diakonov, Talk given at International School of Physics, 'Enrico Fermi', Course 80: Selected Topics in Nonperturbative QCD, Varenna, Italy, 1995, hep-ph/9602375.
- [2] T. Banks and A. Casher, Nucl. Phys. B169 (1980) 103.
- [3] P.H. Ginsparg and K.G. Wilson, Phys. Rev. D 25 (1982) 2649.
- [4] T.L. Ivanenko and J.W. Negele, Nucl. Phys. Proc. Suppl. 63 (1998) 504; H.Neff, N.Eicker, T.Lippert, J.W. Negele and K. Schilling, hep-lat/0106016; T. DeGrand, Phys. Rev. D 64 (2001) 094508.
- [5] T. DeGrand and A. Hasenfratz, Phys. Rev. D 64 (2001) 034512.
- [6] M. C. Chu, J. M. Grandy, S. Huang and J. W. Negele, Phys. Rev. D 49 (1994) 6039.
- [7] M.N. Chernodub and V.I. Zakharov, hep-ph/0107130; V.G. Bornyakov, M.N. Chernodub, F.V. Gubarev, M.I. Polikarpov, T. Suzuki, A.I. Veselov and V.I. Zakharov, hep-lat/0103032.
- [8] M. Lüscher and P. Weisz, Commun. Math. Phys. 97 (1985) 59; Erratum: 98 (1985) 433; G. Curci, P. Menotti and G. Paffuti, Phys. Lett. B 130 (1983) 205, Erratum: B 135 (1984) 516.
- [9] M. Alford, W. Dimm, G.P. Lepage, G. Hockney and P.B. Mackenzie, Phys. Lett. B 361 (1995) 87.

- [10] G.P. Lepage and P.B. Mackenzie, Phys. Rev. D 48 (1993) 2250.
- [11] C. Gattringer, M. Göckeler, P.E.L. Rakow, S. Schaefer and A. Schäfer, hep-lat/0105023 (Nucl. Phys. B, in print).
- [12] R. Sommer, Nucl. Phys. B 411 (1994) 839; M. Guagnelli, R. Sommer and H. Wittig, Nucl. Phys. B 535 (1998) 389.
- [13] P. Hasenfratz, Nucl. Phys. B (Proc. Suppl.) 63 (1998) 53; P. Hasenfratz, Nucl. Phys. B 525 (1998) 401; P. Hasenfratz, V. Laliena and F. Niedermayer, Phys. Lett. B 427 (1998) 353.
- [14] P. Hasenfratz, S. Hauswirth, K. Holland, Th. Jörg, F. Niedermayer and U. Wenger, Int. J. Mod. Phys. C 12 (2001) 691.
- [15] R. Narayanan and H. Neuberger, Phys. Lett. B 302 (1993) 62, Nucl. Phys. B 443 (1995) 305.
- [16] C. Gattringer, I. Hip and C.B. Lang, Nucl. Phys. B597 (2001) 451.
- [17] C. Gattringer and I. Hip, Phys. Lett. B 480 (2000) 112.
- [18] C. Gattringer, Phys. Rev. D 63 (2001) 114501.
- [19] S. Itoh, Y. Iwasaki and T. Yoshie, Phys. Rev. D36 (1987) 527, Phys. Lett. B 184 (1987) 375.
- [20] C. Gattringer and C.B. Lang, work in preparation; C. Gattringer, M. Göckeler, C.B. Lang, P.E.L. Rakow, S. Schaefer and A. Schäfer, hep-lat/0110015.
- [21] D.C. Sorensen, SIAM J. Matrix Anal. Appl. 13 (1992) 357; R. B. Lehoucq, D.C. Sorensen and C. Yang, ARPACK User's Guide, SIAM, New York, 1998.
- [22] T. Guhr, A. Müller-Groeling and H. A. Weidenmüller, Phys. Rept. 299 (1998) 189; M.E. Berbenni-Bitsch, S. Meyer, A. Schäfer, J.J.M. Verbaarschot and T. Wettig, Phys. Rev. Lett. 80 (1998) 1146; J.C. Osborn and J.J.M. Verbaarschot, Phys. Rev. Lett. 81 (1998) 268; R. G. Edwards, U. M. Heller, J. Kiskis and R. Narayanan, Phys. Rev. Lett. 82 (1999) 4188; P.H. Damgaard, U.M. Heller and A. Krasnitz, Phys. Lett. B 445 (1999) 366; M. Göckeler, H. Hehl,

- P.E.L. Rakow, A. Schäfer and T. Wettig, Phys. Rev. D 59 (1999) 094503; M.E. Berbenni-Bitsch et al., Phys. Lett. B 438 (1998) 14.
- [23] R.G. Edwards, U.M. Heller, J.E. Kiskis and R. Narayanan, Phys. Rev. D 61 (2000) 074504.
- [24] C. Gattringer, M. Göckeler, C.B. Lang, P.E.L. Rakow and A. Schäfer, hep-lat/0108001.
- [25] I.A. Fox, M.L. Laursen, G. Schierholz, J.P. Gilchrist and M. Göckeler, Phys. Lett. B158 (1985) 332.
- [26] M. Göckeler, P.E.L. Rakow, A. Schäfer, W. Söldner and T. Wettig, Phys. Rev. Lett. 87 (2001) 042001.
- [27] I. Horváth, N. Isgur, J. McCune and H. B. Thacker, hep-lat/0102003.
- [28] T. De Grand and A. Hasenfratz, hep-lat/0103002; I. Hip, Th. Lippert, H. Neff, K. Schilling and W. Schroers, hep-lat/0105001; R.G. Edwards and U.M. Heller, hep-lat/0105004; T. Blum, N. Christ, C. Cristian, C. Dawson, X.Liao, G. Liu, R. Mawhinney, L. Wu and Y. Zhestkov, hep-lat/0105006.